

A Novel Hyperbolic Two-Dimensional Carbon Material with an In-Plane Negative Poisson's Ratio Behavior and Low-Gap Semiconductor Characteristics

Mengyang Li,[#] Kun Yuan,^{*,#} Yaoxiao Zhao,[#] Zhibin Gao,^{*} and Xiang Zhao^{*}



Cite This: *ACS Omega* 2020, 5, 15783–15790



Read Online

ACCESS |



Metrics & More

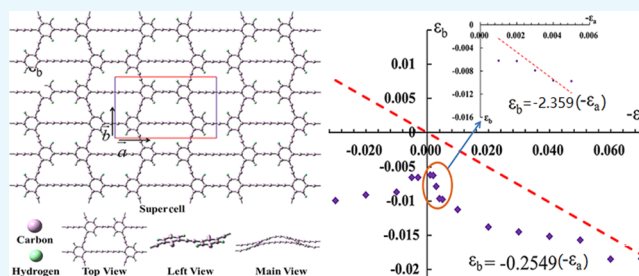


Article Recommendations



Supporting Information

ABSTRACT: Poisson's ratio is one of the fundamental features of materials, reflecting the transverse strain response to the applied certain axial strain. The materials with a negative Poisson's ratio, also known as auxetic materials, are rare in nature and attract lots of research interest because of their unusual mechanical behavior and extensive applications in mechanical nanodevices. Here, we proposed and studied a novel hyperbolic two-dimensional graphene-like structure (GLS) showing a negative Poisson's ratio behavior by first-principles calculation. The thermodynamic, dynamic, lattice dynamic, and mechanical stabilities of the GLS were carefully studied. In addition, we also explored the electronic structure, mechanical characteristics, and optical-electronic characteristics. The GLS not only displays a negative Poisson's ratio in certain directions but also shows low-gap semiconductor characteristics and superior electronic conductivity. It is a potential sunscreen material because of the outstanding reflection and absorption for ultraviolet and infrared light.



1. INTRODUCTION

Poisson's ratio is one of the fundamental parameters of a mechanical property of materials, which reflects the transverse strain response to the applied uniaxial load.^{1,2} The Poisson's ratio is defined as $\nu_{ab} = -\varepsilon_b/\varepsilon_a$, where ε_a is an applied strain along the a direction and ε_b is the resulting strain in the transverse b direction.^{3–6} Generally, materials are prone to expand (contract) in a perpendicular direction when a compressive (tensile) strain is performed in one certain direction, resulting in a positive Poisson's ratio.^{7,8} In addition, previous studies verified that the Poisson's ratios of elastic materials generally fall in the range of $0 < \nu < 0.5$.^{9–12} Notably, there are several materials with a negative Poisson's ratio (NPR), which are allowable in elastic theory and rare in nature.^{9,10} The NPRs for materials mean that the materials will expand under stretching, and they will contract when there is compressive stress. Materials with a NPR are known as auxetic materials, exhibiting unusual mechanical behaviors and rendering them much more promising applications in mechanical nanodevices.^{11,12} Foams with negative Poisson's ratios were first produced from conventional low-density open-cell polymer foams by causing the ribs of each cell to permanently protrude inward in 1987.¹³

Primeval NPR phenomena are generally observed in engineered three-dimensional (3D) bulk structures, including natural and man-made materials. Many cubic metals^{14,15} and α -cristobalite¹⁶ are reported to show NPR behaviors. Especially, the NPRs of some materials are derived from the phase transition.^{17–20} In addition, special structures are also

engineered to obtain NPRs, such as microporous polymers,^{21,22} molecular networks,^{23,24} reentrant foams,^{13,25} or honeycomb,^{26–29} hierarchical structures,³⁰ special origami structures,^{31–33} and 3D hinged structures.^{34–38} The unusual auxetic effect and concomitant enhancements in material properties offer enormous potential applications in many technologically important fields, such as biomedicine, sensors, fasteners, and protective equipment.^{8,39} Thus, the design and synthesis of multifunctional auxetic materials are urgently desired.

Although two-dimensional (2D) auxetic materials are rather rare in nanomaterials, they attract extensive research interest because of their novel properties, such as enhanced toughness and sound or vibration absorption.³⁹ Furthermore, the acknowledged 2D auxetic materials include monolayer Be_3C_2 ,⁴⁰ black phosphorus,¹ BP,⁴¹ SnSe,⁴² penta-graphene,⁴³ silicon dioxide,¹² borophene,⁴⁴ TiN,⁴⁵ MX_2 ($M = \text{Mo}, \text{W}, \text{Tc}, \text{Re}; X = \text{S}, \text{Se}, \text{Te}$)³ and ABP_6X_6 ($A = \text{Ag}, \text{Cu}; B = \text{Bi}, \text{In}; X = \text{S}, \text{Se}$).⁴⁶ The NPR for most of the 2D auxetic materials is derived from its reentrant, hinged geometric structures, chemical compositions, and electronic structures.^{3,10,12} Specifically, the NPR of well-known black phosphorene is -0.027 , resulting from its puckered

Received: January 14, 2020

Accepted: June 4, 2020

Published: June 25, 2020



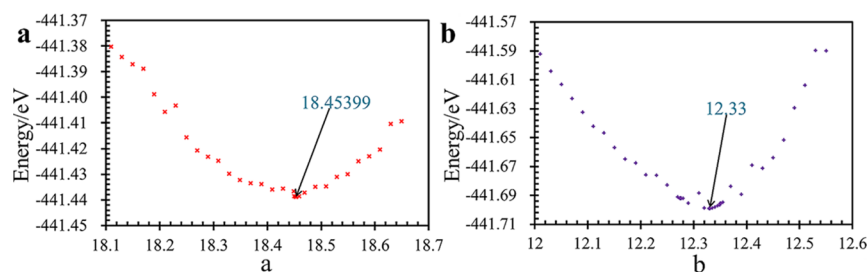


Figure 1. Optimization of lattice parameters along the (a) *a* direction and (b) *b* direction with a constant of the *c* direction (25 Å).

configurations, and luckily is confirmed by both theoretical and experimental methods.⁴¹ Notably, the reported largest NPR among 2D auxetic materials is -0.267 for monolayer δ -P. The NPRs of other 2D materials are relatively small. In addition, the 2D materials show the out-of-plane and in-plane NPRs. For example, one state-of-the-art theoretical calculation predicted that monolayer ABP_6X_6 ($A=Ag, Cu; B=Bi, In; X=S, Se$) are to a new class of auxetic materials with an out-of-plane NPR.⁴⁶ However, a novel auxetic material, penta-silicene, is recently reported with an in-plane NPR.⁴⁷

Up to now, 2D materials still attract lots of research interest since the discovery of well-known graphene⁴⁸ because they show various excellent properties with many potential applications in electronics, optoelectronics, and energy conversion.⁴⁹ For example, 2D BN and MoS_2 have much higher piezoelectricity, and thus they are beneficial for efficient mechanical-to-electrical energy conversion.^{50,51} The black phosphorene with an NPR shows excellent ferroelasticity and is a candidate for nonvolatile memory devices. Taking together, 2D materials display lots of excellent features, and auxetic materials also show unique mechanical properties. The unusual auxetic behavior in combination with other remarkable properties of 2D materials will lead to novel multifunctionalities.^{45,52} Thus, it is highly recommended to design and synthesize special functionalized 2D materials simultaneously with NPRs.

Geometric considerations are predominantly reported in the literature to understand the auxetic phenomenon and design novel auxetic materials.^{7,8} Herein, we proposed a novel 2D material with a hyperbolic geometry, called graphene-like structure (GLS), via state-of-the-art theoretical calculations. The GLS shows an interesting anisotropy NPR behavior and semiconductor characteristics. The values of NPRs depend on the orientation of applied strain. In addition, a slightly small band gap for the GLS indicates excellent electronic mobility, meaning a promising application in the electronic devices. Furthermore, the GLS is the first 2D structure with a hyperbolic geometry leading to an interesting NPR behavior and some excellent properties. This new mechanism of the auxetic phenomenon will extend the scope of auxetic nanomaterials and can serve as principles for future design of auxetic materials. We hope that these interesting findings would motivate further experimental and theoretical efforts to 2D materials with excellent auxetic behaviors.

2. COMPUTATIONAL METHODS

All of the first-principles calculations were carried out based on the Kohn–Sham density functional theory (DFT) with the Vienna *ab initio* simulation package (VASP).^{53–55} The generalized gradient approximation as parameterized by Perdew, Burke, and Ernzerhof (PBE) for exchange–correlation functional is used to relax the geometries.⁵⁶ The plane-wave

basis set with a kinetic energy cutoff of 400 eV is used to expand the valence electron wave functions. The convergence criterions for the energy in electronic SCF iterations and the force in ionic step iterations are 1.0×10^{-6} and 5.0×10^{-2} , respectively. The non-periodic direction was set along the *c* direction, and an at least 20 Å vacuum slab was added in order to eliminate the interactions between the layers of GLS. The reciprocal space is sampled with *k*-grid densities of 331, 551, 771, and 991, and finally a *k* point of 771 was selected with consideration of accuracy and efficiency. Furthermore, the geometries and electronic density for conduction band minimum (CBM) and valence band maximum (VBM) of the GLS were conducted with VESTA software.⁵⁷

The Poisson's ratio of the GLS was calculated from its definition $\nu_{ab} = -\epsilon_b/\epsilon_a$, where $\epsilon_a = \Delta L_a/L_{a0}$ is an applied strain along the *a* direction and $\epsilon_b = \Delta L_b/L_{b0}$ is the resulting stress in the transverse *b* direction. In our calculations of uniaxial strain (for example, along the *a* direction), the lattice constant L_a of the *a* direction was manually set and fixed, and then the lattice constant L_b was obtained via optimizing the structure, which corresponds to the lowest energy of the considered system. Finally, the Poisson's ratio ν can be obtained in each strain percentage.

3. RESULTS AND DISCUSSIONS

3.1. Stability of the GLS. First, the optimization of the lattice parameters (*a* and *b* directions) with a constant *c* of 25 Å was carried out. As shown in Figure 1a,b, the results of the relationship between the potential energies and the changing *a* and *b* parameters indicate that the optimal lattice parameters of the GLS ($C_{48}H_8$) for *a* and *b* directions are 18.45 and 12.33 Å, respectively. The geometry of the GLS belongs to the P_1 point group (space group no. 1) with much lower symmetry. In addition, the geometry of the GLS is shown in Figure 2. The novel hyperbolic configuration of the GLS can be seen from the left view and main view. The applications of molecules are determined by their features, which seriously rely on the geometries. A previous work on polymerized phenanthrene molecules forming porous graphene had shown a tunable Poisson's ratio on the nanoscale.⁵⁸ Thus, it is inferred that the GLS with a unique hyperbolic configuration possesses interesting Poisson's ratio behaviors, which would be revealed as follows.

In order to evaluate the lattice dynamic stability of the GLS, the phonon bands of the unit cell of the GLS were calculated using VASP combined with Phonopy.^{59,60} As shown in Figure S1, although there are few imaginary frequencies, the maximum imaginary frequency for the unit cell of the GLS is less than 50 cm^{-1} . Considering the huge system and phonon band simulations for the primitive cell of the GLS, we thought that the imaginary frequency in Figure S1 is rational and would be

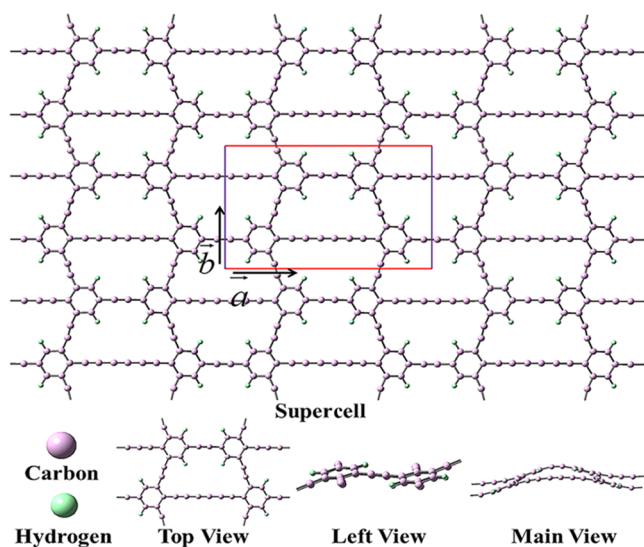


Figure 2. Geometries of a supercell and the top view, left view, and main view of the GLS.

absent when the phonon band calculations were carried out for a supercell of the GLS. Given that any *ab initio* calculations of phonons with high accuracy are far beyond our current computational capabilities, we hope that more researches could explore it. Besides, in the experiment, variable and complex substrate environment and categories would probably further stabilize the GLS.

In addition, the formation energy for molecule is a good method to evaluate the thermodynamic stability. If the formation energy of a compound is negative, this compound will be thermodynamically stable. The formation energy of the GLS ($C_{48}H_8$) per atom is

$$\Delta E(C_M H_N) = \frac{E(C_M H_N) - M\mu_C - N\mu_H}{M + N}$$

where $\Delta E(C_M H_N)$ is the formation energy per atom of $C_{48}H_8$, $E(C_M H_N)$ is the total energy (-441.697 eV) of $C_M H_N$ calculated on PBE, and chemical potentials (μ_C and μ_H) of C and H atoms are the cohesive energies of graphene (-7.906 eV) and one-dimensional metallic hydrogen (-1.75 eV), respectively.^{61,62} The formation energy of $C_{48}H_8$ is -0.861 eV/atom, implying that the GLS is thermodynamically stable.

Furthermore, for any mechanically stable 2D materials, a necessary but not a sufficient condition must be satisfied: $C_{11}C_{22} - C_{12}^2 > 0$ and $C_{66} > 0$.^{12,47,63} The stiffness matrix of the GLS is given in Table S1. Especially, the calculated four elastic stiffness constants of GLS are $C_{11} = -100.85$ GPa, $C_{22} = -63.04$ GPa, $C_{12} = -12.73$ GPa, and $C_{66} = -6.80$ GPa. Clearly, the results of $C_{11}C_{22} - C_{12}^2 > 0$ with slightly negative C_{66} verified the defective mechanical stability of the GLS. Again, the low stability originates from the absence of a proper substrate or chemical environment. The previous reports also demonstrated that materials with negative shear moduli would be stable if confined.^{64,65} Furthermore, we also calculated the Young's modulus of the GLS, and comparing with the Young's modulus of other 2D materials, including graphene (1023 GPa), BP ($E_x = 168$ GPa, $E_y = 38$ GPa), and α -2D silica (178.56 GPa),¹² there are some deviations between the Young's modulus of the GLS and the values of classical 2D materials due to the defective mechanical stability. In the future, we will try to remold and

stabilize the GLS with hydrogenation or other chemical modifications.

Furthermore, the dynamic stability of the GLS was also explored with molecular dynamics, and the relationship between the changing potential energy and increasing time within 3 ps is shown in Figure 3. After carefully checking the dynamic data, the

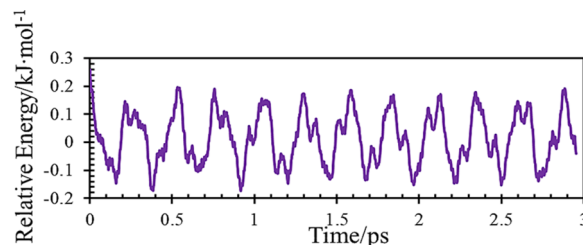


Figure 3. Relationship between the potential energy and time.

maximum energy difference is 0.43 kJ/mol, which means that the structure of the GLS would hardly fluctuate with changing time. In other words, the GLS shows good dynamic stability.

According to the above discussion on the stability of the GLS, we thought that the GLS would be a potential 2D material with interesting mechanic features. Although there is experimental information on the GLS proposed in the present work, there are several reasonable experimental methods, including chemical vapor deposition (CVD),⁶⁶ close-spaced vapor transport (CVT),⁶⁷ flux growth,⁶⁸ high-pressure flux method,⁶⁹ and epitaxial growth,⁷⁰ proposed to generally synthesize 2D materials. All of these general experimental methods will be the promising candidates to synthesize the GLS theoretically proposed here with a hyperbolic structure.

3.2. Electronic Structures of the GLS. As shown in Figure 4, the energy eigenvalues of VBM and CBM for the GLS are -0.40 and 0.38 eV, respectively. There is no energy level traversing the Fermi level, and a band gap of GLS is 0.78 eV with weak semiconductor features at the PBE level, indicating that the

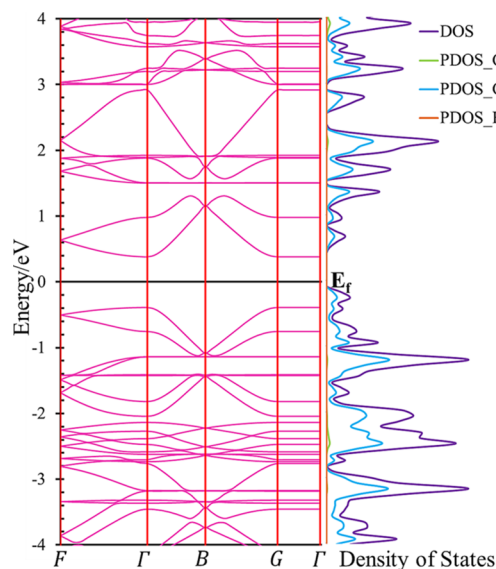


Figure 4. Energetical band structure of the GLS along high symmetry points and the density of states, the partial density states of s and p orbitals of carbon atoms, and the partial density state of s orbitals of hydrogen atoms.

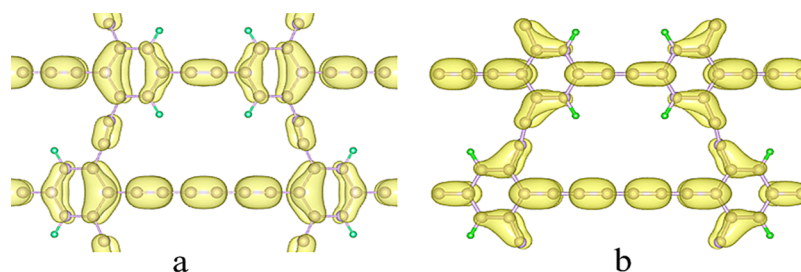


Figure 5. Population of the electronic density for (a) valence band maximum (VBM) and (b) conduction band minimum (CBM).

GLS has a potential application for designing the nano-electro-optical devices with infrared absorption. A small band gap of 0.66 eV also occurs in δ -P.⁷¹ In addition, there are also several 2D materials with NPR behaviors showing semiconductor features.⁴⁶ Furthermore, the total density of states (DOS) and partial density of states (PDOS) are shown in Figure 4. We considered the contributions of s and p orbitals of carbon and s orbitals of hydrogen to DOS. It is clear that the main contribution for DOS is from the p orbitals of carbon atoms. Around the E_b the p orbital contributes significantly, indicating the origin of the semiconducting behavior of the GLS.

Similarly, VBM and CBM are mainly contributed by p orbitals of carbon atoms. As shown in Figure 5a,b, the populations of VBM and CBM cover all of the molecules with several nodes. Thus, there is no clear difference between electrons and holes, which is consistent with a small band gap. These nodes represent the alternative triple and single bonds along the whole carbon skeleton. The alternative triple and single bonds are also confirmed by bond lengths of 1.21 and 1.40 Å for the carbon skeleton except for benzene. The benzenes in the GLS show a little distortion, although six carbon atoms are in the same plane. Specifically, a bond length of 1.40/1.44 Å is for benzene, and it is clearly distinguished for the standard benzene with 1.40 Å, attributing to unequal carbon atoms.

3.3. Mechanical Properties of the GLS. Clearly, as shown in Figure 2, the GLS possesses features of hyperbolic geometry and reentrant polygon, which will lead to an NPR behavior. In the ab plane, the geometry of the GLS consists of reentrant hexagons, one of the present configurations for auxetic materials. In addition, the geometry of the GLS shows layered and wave configurations in the bc plane and ac plane, respectively. The thickness of the GLS is around 3.10 Å. Due to these unique geometrical features, the GLS possesses unique mechanical properties.

The relationship between $-\varepsilon_a$ and ε_b is shown in Figure 6, where ε_a (ε_b) is the applied strain along the a (b) direction and $-\varepsilon_b$ ($-\varepsilon_a$) is the resulting strain along the b (a) transverse a (b) direction. As shown in Figure 6, Poisson's ratio phenomena of the GLS are complex along different directions, leading to distinguished Poisson's ratio, which coincides with the anisotropy of the GLS. Clearly, when the GLS is stretched along the a direction, as shown in Figure 6a, the GLS shows a positive Poisson's ratio. However, the GLS shows characteristics of auxetic materials when it is compressed along the a direction, indicating an interesting mechanical behavior of the GLS. The result of linear fitting within 0.1–10% tension reveals that the NPR of the GLS is -0.25 ($\nu_a(-) = -0.25$). Notably, the NPR of the GLS is -2.36 when the tension is within 0.1–0.5% along the a direction. This interesting NPR behavior is similar with the graphene, in which the Poisson's ratio evolves from positive to negative when the applied tensile strain exceeds about 6%.⁷²

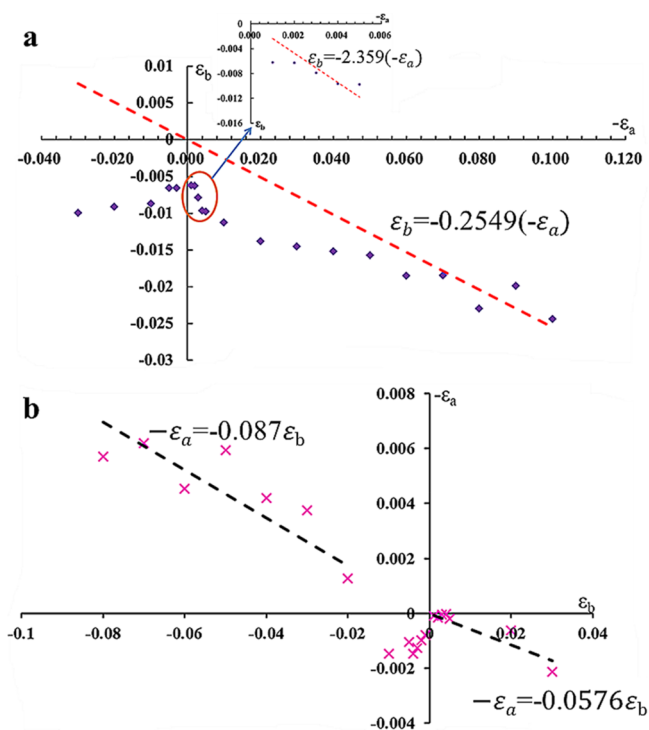


Figure 6. Relationships (a) between applied strain $-\varepsilon_a$ along the a direction and strain ε_b along the b direction and (b) between applied strain ε_b along the b direction and strain $-\varepsilon_a$ along the a direction.

Remarkably, the NPR of the GLS along the a direction with tension is quite higher compared with penta-graphene ($\nu = -0.068$),⁴³ borophene ($\nu_x = -0.04, \nu_y = -0.02$),^{44,52} Be_5C_2 ($\nu_x = -0.04, \nu_y = -0.16$),⁴⁰ HfB_2 ($\nu_y = -0.174$), VB_2 ($\nu_y(-) = -0.253$), and TaB_2 ($\nu_y = -0.224$).¹⁰

Here, we also applied constraint uniaxial strain, within -8% to $+3\%$, along the b direction for investigating the anisotropic mechanical properties. As shown in Figure 6b, the GLS presents a lower NPR for both compressive and tensile strains along the b direction. The result of linear fitting reveals that the values of NPRs for GLS along the b direction are around -0.0576 to -0.087 , which are similar to penta-graphene ($\nu = -0.068$),⁴³ though there are positive Poisson's ratios when the compressive strain along the b direction is less than 2%. Clearly, the mechanical property of the GLS is complex.

Generally, the Poisson's ratios of the material with the reentrant structure are functions of the strains, especially for the large deformation, instead of a constant. Therefore, the relationship between the Poisson's ratios and the strains is shown in Figure S2. It can be seen that with increasing the compressive strain along the a direction from 0.1 to 2%, the NPR drastically decreases from -6.208 to -0.691 . Consequently, it

converges to a constant value of -0.26 with the compressive strain (ε_a) further increasing (Figure S2 a). The relationship between the Poisson's ratios and the strains along the b direction (ε_b) is much more complicated. Roughly, the Poisson's ratios are of small negative values in the regions of higher compressive strains with $|\varepsilon_b| > 20\%$ and those of tensile strains $\varepsilon_b > 0$, while in the small value of compressive strains ($|\varepsilon_b| > 10\%$), the Poisson's ratios are positive (Figure S2b).

Although the whole negative Poisson's ratio of the 2D GLS is not good enough, there are still evident negative Poisson's ratio (NPR) effects along the given directions. Yu et al.³ revealed that the differences between NPRs along different directions represent an anisotropy auxetic material in 2017. Besides, our result is similar to single-layer graphene, which shows a positive Poisson's ratio at a small strain while a negative Poisson's ratio at a large strain.⁷² Therefore, it can be induced that the GLS with a hyperbolic geometry also shows an anisotropy Poisson's ratio, which shows different behaviors along a certain direction. The hyperbolic configuration, which results in similar NPR behaviors derived from the reentrant and hinged geometries, is still expected to be a second key factor for a novel 2D material with NPR performance. In detail, the hinged structures will lead to changes in the material stiffness, and the magnitude of the Poisson's ratio increases as the contrast between the unit cell stiffness increases. Furthermore, the increasing stiffness will enhance the deformation along one certain direction but inhibit the deformation along another direction, which is the main cause behind the achieved Poisson's ratio of hinged structures.⁷³ This novel hyperbolic structure with the auxetic phenomenon will extend the scope of auxetic nanomaterials.

It is known that the negative Poisson's ratio of nanostructures and even metamaterials originates from the hidden degree of freedom (DOF). Those DOF parameters are hinged bonds (angles) and rotated bonds (angles). This hidden DOF can be released by the external strain, lifted temperature, pressure, and volume.^{8,12,58} The negative Poisson's ratio of our GLS is derived from the warping effect of carbon ribbons. An external strain could release the hidden degree of freedom when the system possesses buckling and warping.⁷¹ Furthermore, a previous report showed that chemical functionalization could enhance the auxeticity of graphene. Also, it is notable to expect more excellent auxetic nanomaterials with a hyperbolic configuration and suitable chemical functionalization.¹¹ In order to clearly show the mechanism of NPRs for the GLS, we plot the local skeleton geometry of the GLS, as shown in Figure S3. The detailed structural information is shown in Table S2, including one optimal GLS without strain, which would be compared with, for example, two deformations of GLS with 30% strain along a and b , respectively. According to Table S2, while there are applied strain along a , the negative Poisson's ratio of the GLS is derived from the change of dihedral angle for C17–C18–C19–C20 and C9–C10–C11–C12. In other words, the dihedral angles rather than the bond length along b stretch under a tensile force along a , which is the similar case for the auxetic materials semi-fluorinated graphene and δ -phosphorene.^{11,68} Furthermore, the negative Poisson's ratio of the GLS along b originated from the slight change of the bond lengths of C13–C14, C14–C15, and C15–C16 and the change of the bond angles of C13–C14–C15 and C14–C15–C16.

3.4. Optical and Electronic Properties of the GLS. As a multifunctional material, we also explored the optical and electronic properties of the GLS. The dielectric function of the material is defined as $\varepsilon(\omega) = \varepsilon_1(\omega) + i\varepsilon_2(\omega)$, with the real part

($\varepsilon_1(\omega)$) and imaginary part ($\varepsilon_2(\omega)$),⁷⁴ when there is electromagnetic radiation. The relationships between the dielectric function and energy of electromagnetic radiation along different directions are shown in Figure 7.

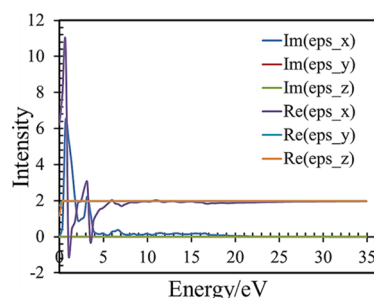


Figure 7. Relationships between the real part and imaginary part of the dielectric function for the GLS and energy of electromagnetic waves.

According to the results of the dielectric function, we also obtained the electronic conductivity, refractive index, reflective index, and absorption index of the GLS along three orthometric directions.⁷⁵ As shown in Figure 8a, the GLS has a better electronic conductivity when the wavelength and energy of electromagnetic waves are long and short, respectively. Nevertheless, the electronic conductivity is weak and tends to a constant with the value of energy (>21 eV).

The relationships between the refractive index and the energy (wavelength) of electromagnetic waves agree well with the normal rule for ideal 2D materials (Figure 8b).⁷⁶ As shown in Figure 8b, when the energy is lower than 7 eV, the refractive index of the GLS seriously fluctuates along a normal vector and has three maximal values and two minimal values. The maximum value of the refractive index is close to 1.0, and the minimum value of the refractive index tends to 0. In addition, the refractive index along three directions tends to 0.25.

The different variation tendencies for the reflectivity of the GLS with the changing incident energy are shown in Figure 8c. In the plane of the GLS, the reflectivity of the GLS is much lower, and the changing tendency along x (a) and y (b) directions coincides with each other. In other words, the performances of the reflectivity of the GLS along x and y directions show similar changes. However, there are two maximum values of reflectivity along the normal vector at around the near-infrared region (1.5 eV) and ultraviolet region (3.5 eV). The reflectivities of the GLS are close to 1 and 0.6 at 1.5 and 3.5 eV, respectively. It is thus clear that there are ideal reflection functions at certain infrared and ultraviolet wavelengths, which coincide with the small band gap, confirming that the GLS and δ -P⁷¹ have a potential application for designing the electro-optical devices with infrared absorption.

Figure 8d also shows the relationship between absorption index and changing radiation energy. The similar changes for absorption index and reflectivity are presented. At 1.5 eV of the infrared region and 3.5 eV of the ultraviolet region, there are two maximum absorptions. Notably, the absorption intensity of the GLS within the visible region is clearly lower than those within infrared and ultraviolet regions. Additionally, when the incident wavelength is less than 275 nm, there is no absorption. Thereby, the GLS is not suitable for a visible light absorption material.

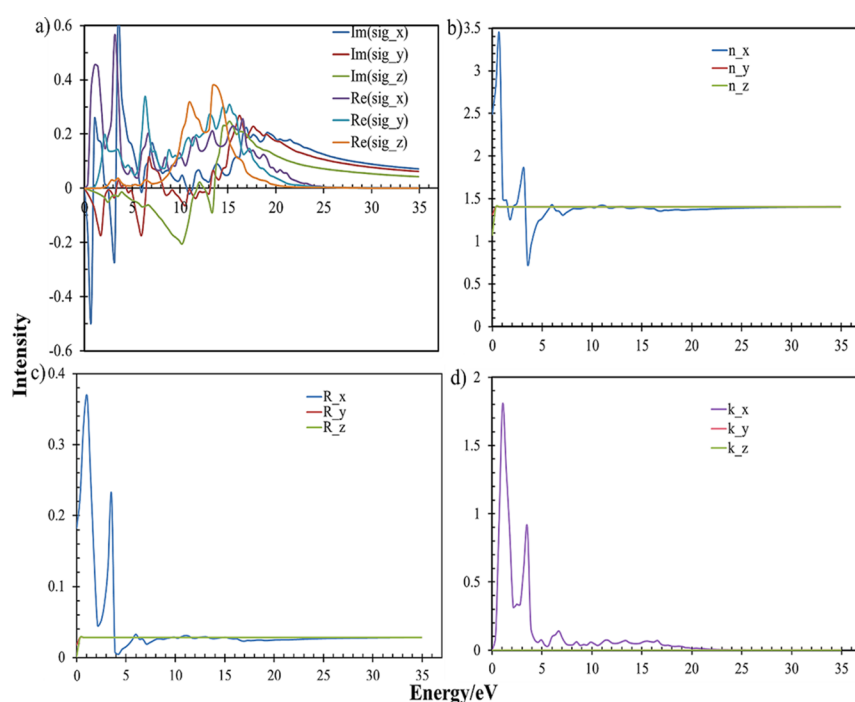


Figure 8. (a) Relationship between the real (Re) and imaginary (Im) parts of electronic conductivity and the energy of electromagnetic waves along three orthometric directions for the GLS. (b) Relationship between refractive index and the energy of electromagnetic waves along three orthometric directions for the GLS. (c) Relationship between reflectivity and the energy of electromagnetic waves along three orthometric directions for the GLS. (d) Relationship between absorption index and radiation energy along three orthometric directions for the GLS.

4. CONCLUSIONS

We proposed a novel 2D material (GLS) with a hyperbolic configuration via state-of-the-art theoretical methods, and the results confirm that the GLS has excellent thermodynamic and dynamic stabilities as well as acceptable lattice dynamic and defective mechanic stabilities. The GLS with a small band gap of 0.78 eV exhibits semiconductor characteristics, meaning that the GLS has a potential application for designing the nano-electro-optical devices with infrared absorption as well as δ -P. The density of states and partial density of states show that the valence band maximum and conduction band minimum are mainly from p orbitals of carbon atoms. The GLS shows an interesting negative Poisson's ratio behavior along certain directions due to the novel hyperbolic configuration. This kind of hyperbolic configuration is expected to be a novel geometry leading to negative Poisson's ratios of materials and a second principle for future designing auxetic materials. In addition, the GLS has an ideal electronic conductivity depending on the wavelength and can absorb and reflect the certain wavelength of ultraviolet and infrared light. Accordingly, we highly expect that these interesting findings would motivate further theoretical and experimental efforts in 2D auxetic carbon nanomaterials.

Associated Content

■ ASSOCIATED CONTENT

Supporting Information

The Supporting Information is available free of charge at <https://pubs.acs.org/doi/10.1021/acsomega.0c00182>.

Phonon band of the unit cell of GL, stiffness matrix of GL coefficients, geometry of GLS for the NPR mechanism study, the relationship between the Poisson's ratios and the strains along a (and b directions, and the geometrical

parameters of GLS shown in Figure S3 without strain (GLS_0) and deformation of GLS with strain along a (GLS_a) and b (GLS_b), respectively (PDF)

■ AUTHOR INFORMATION

Corresponding Authors

Kun Yuan – School of Chemical Engineering and Technology, Key Laboratory for New Molecule Materials Design and Function of Gansu Universities, Tianshui Normal University, Tianshui 741001, China; orcid.org/0000-0001-5552-4424; Email: yuankun@tsnu.edu.cn

Zhibin Gao – Department of Physics, National University of Singapore, Singapore 117551, Republic of Singapore; orcid.org/0000-0002-6843-381X; Email: zhibin.gao@nus.edu.sg

Xiang Zhao – Institute for Chemical Physics & Department of Chemistry, School of Science, State Key Laboratory of Electrical Insulation and Power Equipment & MOE Key Laboratory for Nonequilibrium Synthesis and Modulation of Condensed Matter, Xi'an Jiaotong University, Xi'an 710049, China; orcid.org/0000-0003-3982-4763; Email: xzhao@mail.xjtu.edu.cn

Authors

Mengyang Li – Institute for Chemical Physics & Department of Chemistry, School of Science, State Key Laboratory of Electrical Insulation and Power Equipment & MOE Key Laboratory for Nonequilibrium Synthesis and Modulation of Condensed Matter, Xi'an Jiaotong University, Xi'an 710049, China

Yaoxiao Zhao – Institute for Chemical Physics & Department of Chemistry, School of Science, State Key Laboratory of Electrical Insulation and Power Equipment & MOE Key Laboratory for Nonequilibrium Synthesis and Modulation of Condensed Matter, Xi'an Jiaotong University, Xi'an 710049, China

Complete contact information is available at:
<https://pubs.acs.org/10.1021/acsomega.0c00182>

Author Contributions

*M.Y.L., K.Y., and Y.X.Z. contributed equally to this work.

Notes

The authors declare no competing financial interest.

ACKNOWLEDGMENTS

This work was supported by the National Natural Science Foundation of China (21663024 and 21773181). K.Y. acknowledges the financial support from the “Feitian” Scholar Program of Gansu Province, Chunhui Program of the Chinese Ministry of Education, Longyuan Youth Talent Innovative Support Program of Gansu Province. Z.G. acknowledges the financial support from MOE tier 1 funding, Singapore (grant no. R-144-000-402-114). The authors thank Dr. Pei Zhao of the Institute of Molecular Science of Japan for the help on the calculation of optical and electronic properties of GLS.

REFERENCES

- (1) Jiang, J.-W.; Park, H. S. Negative Poisson's ratio in single-layer black phosphorus. *Nat. Commun.* **2014**, *5*, 4727.
- (2) Kou, L.; Chen, C.; Smith, S. C. Phosphorene: Fabrication, properties, and applications. *J. Phys. Chem. Lett.* **2015**, *6*, 2794–2805.
- (3) Yu, L.; Yan, Q.; Ruzsinszky, A. Negative Poisson's ratio in 1T-type crystalline two-dimensional transition metal dichalcogenides. *Nat. Commun.* **2017**, *8*, 15224.
- (4) Rouxel, T. Elastic properties and short-to medium-range order in glasses. *J. Am. Ceram. Soc.* **2007**, *90*, 3019–3039.
- (5) Mott, P. H.; Roland, C. M. Limits to Poisson's ratio in isotropic materials—general result for arbitrary deformation. *Phys. Scr.* **2013**, *87*, No. 055404.
- (6) Landau, L. D.; Lifshitz, E. M. *Theory of elasticity*; 3rd edition, Pergamon/Oxford: 1986.
- (7) Gercek, H. Poisson's ratio values for rocks. *Int. J. Rock Mech. Min. Sci.* **2007**, *44*, 1–13.
- (8) Greaves, G. N.; Greer, A. L.; Lakes, R. S.; Rouxel, T. Poisson's ratio and modern materials. *Nat. Mater.* **2011**, *10*, 823–837.
- (9) Dagdelen, J.; Montoya, J.; de Jong, M.; Persson, K. Computational prediction of new auxetic materials. *Nat. Commun.* **2017**, *8*, 323.
- (10) Zhang, C.; He, T.; Matta, S. K.; Liao, T.; Kou, L.; Chen, Z.; Du, A. Predicting novel 2D MB₂ (M = Ti, Hf, V, Nb, Ta) monolayers with ultrafast dirac transport channel and electron-orbital controlled negative Poisson's ratio. *J. Phys. Chem. Lett.* **2019**, *10*, 2567–2573.
- (11) Qin, R.; Zheng, J.; Zhu, W. Sign-tunable Poisson's ratio in semi-fluorinated graphene. *Nanoscale* **2017**, *9*, 128–133.
- (12) Gao, Z.; Dong, X.; Li, N.; Ren, J. Novel two-dimensional silicon dioxide with in-plane negative Poisson's ratio. *Nano Lett.* **2017**, *17*, 772–777.
- (13) Lakes, R. Foam structures with a negative Poisson's ratio. *Science* **1987**, *235*, 1038–1040.
- (14) Milstein, F.; Huang, K. Existence of a negative Poisson ratio in fcc crystals. *Phys. Rev. B* **1979**, *19*, 2030–2033.
- (15) Baughman, R. H.; Shacklette, J. M.; Zakhidov, A. A.; Stafström, S. Negative Poisson's ratios as a common feature of cubic metals. *Nature* **1998**, *392*, 362–365.
- (16) Yeganeh-Haeri, A.; Weidner, D. J.; Parise, J. B. Elasticity of α -cristobalite: A silicon dioxide with a negative Poisson's ratio. *Science* **1992**, *257*, 650–652.
- (17) Dong, L.; Stone, D. S.; Lakes, R. S. Softening of bulk modulus and negative Poisson ratio in barium titanate ceramic near the Curie point. *Philos. Mag. Lett.* **2010**, *90*, 23–33.
- (18) Hirotsu, S. Elastic anomaly near the critical point of volume phase transition in polymer gels. *Macromolecules* **1990**, *23*, 903–905.
- (19) Hirotsu, S. Softening of bulk modulus and negative Poisson's ratio near the volume phase transition of polymer gels. *J. Chem. Phys.* **1991**, *94*, 3949–3957.
- (20) Li, C.; Hu, Z.; Li, Y. Poisson's ratio in polymer gels near the phase-transition point. *Phys. Rev. E* **1993**, *48*, 603–606.
- (21) Caddock, B. D.; Evans, K. E. Microporous materials with negative Poisson's ratios I. Microstructure and mechanical properties. *J. Phys. D: Appl. Phys.* **1989**, *22*, 1877–1882.
- (22) He, C.; Liu, P.; Griffin, A. C. Toward negative Poisson ratio polymers through molecular design. *Macromolecules* **1998**, *31*, 3145–3147.
- (23) Ortiz, A. U.; Boutin, A.; Fuchs, A. H.; Coudert, F.-X. Anisotropic elastic properties of flexible metal-organic frameworks: How soft are soft porous crystals. *Phys. Rev. Lett.* **2012**, *109*, 195502.
- (24) Evans, K. E.; Nkansah, M. A.; Hutchinson, I. J.; Rogers, S. C. Molecular network design. *Nature* **1991**, *353*, 124–124.
- (25) Brandel, B.; Lakes, R. S. Negative Poisson's ratio polyethylene foams. *J. Mater. Sci.* **2001**, *36*, 5885–5893.
- (26) Glavan, A. C.; Martinez, R. V.; Subramaniam, A. B.; Yoon, H. J.; Nunes, R. M. D.; Lange, H.; Thuo, M. M.; Whitesides, G. M. Omniphobic “R^F Paper” produced by silanization of paper with fluoroalkyltrichlorosilanes. *Adv. Funct. Mater.* **2014**, *24*, 60–70.
- (27) Lakes, R. Advances in Negative Poisson's Ratio Materials. *Adv. Mater.* **1993**, *5*, 293–296.
- (28) Warren, T. L. Negative Poisson's ratio in a transversely isotropic foam structure. *J. Appl. Phys.* **1990**, *67*, 7591–7594.
- (29) Gibson, L. J.; Ashby, M. F. The mechanics of three-dimensional cellular materials. *Proc. R. Soc. London, Ser. A* **1982**, *382*, 43–59.
- (30) Lakes, R. Materials with structural hierarchy. *Nature* **1993**, *361*, 511–515.
- (31) Wei, Z. Y.; Guo, Z. V.; Dudte, L.; Liang, H. Y.; Mahadevan, L. Geometric mechanics of periodic pleated origami. *Phys. Rev. Lett.* **2013**, *110*, 215501.
- (32) Schenk, M.; Guest, S. D. Geometry of Miura-folded metamaterials. *Proc. Natl. Acad. Sci. U. S. A.* **2013**, *110*, 3276–3281.
- (33) Silverberg, J. L.; Evans, A. A.; McLeod, L.; Hayward, R. C.; Hull, T.; Santangelo, C. D.; Cohen, I. Using origami design principles to fold reprogrammable mechanical metamaterials. *Science* **2014**, *345*, 647–650.
- (34) Rothenburg, L.; Berlin, A. A.; Bathurst, R. J. Microstructure of isotropic materials with negative Poisson's ratio. *Nature* **1991**, *354*, 470–472.
- (35) Baughman, R. H.; Galvão, D. S. Crystalline networks with unusual predicted mechanical and thermal properties. *Nature* **1993**, *365*, 735–737.
- (36) Lakes, R. Deformation mechanisms in negative Poisson's ratio materials: structural aspects. *J. Mater. Sci.* **1991**, *26*, 2287–2292.
- (37) Grima, J. N.; Jackson, R.; Alderson, A.; Evans, K. E. Do zeolites have negative Poisson's ratios. *Adv. Mater.* **2000**, *12*, 1912–1918.
- (38) Ishibashi, Y.; Iwata, M. A microscopic model of a negative Poisson's ratio in some crystals. *J. Phys. Soc. Jpn.* **2000**, *69*, 2702–2703.
- (39) Evans, K. E.; Alderson, A. Auxetic materials: Functional materials and structures from lateral thinking. *Adv. Mater.* **2000**, *12*, 617–628.
- (40) Wang, Y.; Li, F.; Li, Y.; Chen, Z. Semi-metallic Be₅C₂ monolayer global minimum with quasi-planar pentacoordinate carbons and negative Poisson's ratio. *Nat. Commun.* **2016**, *7*, 11488.
- (41) Wang, H.; Li, X.; Sun, J.; Liu, Z.; Yang, J. BP₂ monolayer with multiferroicity and negative Poisson's ratio: a prediction by global optimization method. *2D Mater.* **2017**, *4*, No. 045020.
- (42) Zhang, L.-C.; Qin, G.; Fang, W.-Z.; Cui, H.-J.; Zheng, Q.-R.; Yan, Q.-B.; Su, G. Tinselenidene: A two-dimensional auxetic material with ultralow lattice thermal conductivity and ultrahigh hole mobility. *Sci. Rep.* **2016**, *6*, 19830.
- (43) Zhang, S.; Zhou, J.; Wang, Q.; Chen, X.; Kawazoe, Y.; Jena, P. Penta-graphene: A new carbon allotrope. *Proc. Natl. Acad. Sci. U. S. A.* **2015**, *112*, 2372–2377.
- (44) Wang, H.; Li, Q.; Gao, Y.; Miao, F.; Zhou, X.-F.; Wan, X. G. Strain effects on borophene: ideal strength, negative Poisson's ratio and phonon instability. *New J. Phys.* **2016**, *18*, No. 073016.

- (45) Zhou, L.; Zhuo, Z.; Kou, L.; Du, A.; Tretiak, S. Computational dissection of two-dimensional rectangular titanium mononitride TiN: Auxetics and promises for photocatalysis. *Nano Lett.* **2017**, *17*, 4466–4472.
- (46) Zhang, C.; Nie, Y.; Du, A. Intrinsic ultrahigh negative Poisson's ratio in two-dimensional ferroelectric ABP_2X_6 materials. *Acta Phys.-Chim. Sin.* **2019**, *35*, 1128–1133.
- (47) Gao, Z.; Zhang, Z.; Liu, G.; Wang, J.-S. Ultra-low lattice thermal conductivity of monolayer penta-silicene and penta-germanene. *Phys. Chem. Chem. Phys.* **2019**, *21*, 26033–26040.
- (48) Novoselov, K. S.; McCann, E.; Morozov, S. V.; Fal'ko, V. I.; Katsnelson, M. I.; Zeitler, U.; Jiang, D.; Schedin, F.; Geim, A. K. Unconventional quantum hall effect and Berry's phase of 2π in bilayer graphene. *Nat. Phys.* **2006**, *2*, 177–180.
- (49) Butler, S. Z.; Hollen, S. M.; Cao, L.; Cui, Y.; Gupta, J. A.; Gutiérrez, H. R.; Heinz, T. F.; Hong, S. S.; Huang, J.; Ismach, A. F.; Johnston-Halperin, E.; Kuno, M.; Plashnitsa, V. V.; Robinson, R. D.; Ruoff, R. S.; Salahuddin, S.; Shan, J.; Shi, L.; Spencer, M. G.; Terrones, M.; Windl, W.; Goldberger, J. E. Progress, challenges, and opportunities in two-dimensional materials beyond graphene. *ACS Nano* **2013**, *7*, 2898–2926.
- (50) Wang, K.; Wang, J.; Fan, J.; Lotya, M.; O'Neill, A.; Fox, D.; Feng, Y.; Zhang, X.; Jiang, B.; Zhao, Q.; Zhang, H.; Coleman, J. N.; Zhang, L.; Blau, W. J. Ultrafast saturable absorption of two-dimensional MoS_2 nanosheets. *ACS Nano* **2013**, *7*, 9260–9267.
- (51) Pacilé, D.; Meyer, J. C.; Girit, C. Ö.; Zettl, A. The two-dimensional phase of boron nitride: Few-atomic-layer sheets and suspended membranes. *Appl. Phys. Lett.* **2008**, *92*, 133107.
- (52) Kou, L.; Ma, Y.; Tang, C.; Sun, Z.; Du, A.; Chen, C. Auxetic and ferroelastic borophane: A novel 2D material with negative Poisson's ratio and switchable Dirac transport channels. *Nano Lett.* **2016**, *16*, 7910–7914.
- (53) Kresse, G.; Furthmüller, J. Efficient iterative schemes for *ab initio* total-energy calculations using a plane-wave basis set. *Phys. Rev. B: Condens. Matter Mater. Phys.* **1996**, *54*, 11169–11186.
- (54) Kresse, G.; Furthmüller, J. Efficiency of *ab-initio* total energy calculations for metals and semiconductors using a plane-wave basis set. *Comput. Mater. Sci.* **1996**, *6*, 15–50.
- (55) Kresse, G.; Hafner, J. *Ab initio* molecular-dynamics simulation of the liquid-metal-amorphous-semiconductor transition in germanium. *Phys. Rev. B: Condens. Matter Mater. Phys.* **1994**, *49*, 14251–14269.
- (56) Perdew, J. P.; Burke, K.; Ernzerhof, M. Generalized gradient approximation made simple. *Phys. Rev. Lett.* **1996**, *77*, 3865–3868.
- (57) Momma, K.; Izumi, F. VESTA: a three-dimensional visualization system for electronic and structural analysis. *J. Appl. Crystallogr.* **2008**, *41*, 653–658.
- (58) Gao, Z.; Liu, D.; Tománek, D. Two-dimensional mechanical metamaterials with unusual Poisson ratio behavior. *Phys. Rev. Appl.* **2018**, *10*, No. 064039.
- (59) Togo, A.; Tanaka, I. First principles phonon calculations in materials science. *Scr. Mater.* **2015**, *108*, 1–5.
- (60) Deringer, V. L.; Stoffel, R. P.; Togo, A.; Eck, B.; Meven, M.; Dronskowski, R. *Ab initio* ORTEP drawings: a case study of N-based molecular crystals with different chemical nature. *CrystEngComm* **2014**, *16*, 10907–10915.
- (61) Shin, H.; Kang, S.; Koo, J.; Lee, H.; Kim, J.; Kwon, Y. Cohesion energetics of carbon allotropes: Quantum Monte Carlo study. *J. Chem. Phys.* **2014**, *140*, 114702.
- (62) Palke, W. E. The electronic chemical potential and the H atom in the H_2 molecule. *J. Chem. Phys.* **1980**, *72*, 2511.
- (63) Xinchun, S.; Lakes, R. S. Stability of elastic material with negative stiffness and negative Poisson's ratio. *Phys. Status Solidi B* **2007**, *244*, 1008–1026.
- (64) Wang, Y. C.; Lakes, R. S. Composites with inclusions of negative bulk modulus: extreme damping and negative Poisson's ratio. *J. Compos. Mater.* **2005**, *39*, 1645–1657.
- (65) Shaat, M. Size-dependence of Young's modulus and Poisson's ratio: Effects of material dispersion. *Mech. Mater.* **2019**, *133*, 111–119.
- (66) Sugimoto, H.; Fujii, M.; Imakita, K. Size-controlled growth of cubic boron phosphide nanocrystals. *RSC Adv.* **2015**, *5*, 8427–8431.
- (67) Andrade-Arvizu, J. A.; Gariá-Sánchez, M. F.; Courel-Piedrahita, M.; Santoyo-Morales, J.; Jiménez-Olarte, D.; Albor-Aguilera, M.; Vigil-Galán, O. Pressure induced directional transformations on close spaced vapor transport deposited SnS thin films. *Mater. Des.* **2016**, *110*, 878–887.
- (68) Liu, S.; He, R.; Xue, L.; Li, J.; Liu, B.; Edgar, J. H. Single crystal growth of millimeter-sized monoisotopic hexagonal boron nitride. *Chem. Mater.* **2018**, *30*, 6222–6225.
- (69) Sudare, T.; Mori, C.; Hayashi, F.; Teshima, K. Fabrication of fluorapatite nanocrystal-activated carbon composite by the atmospheric pressure plasma-assisted flux method. *Cryst. Growth Des.* **2018**, *18*, 5763–5769.
- (70) Walsh, L. A.; Hinkle, C. L. van der Waals epitaxy: 2D materials and topological insulators. *Appl. Mater. Today* **2017**, *9*, 504–515.
- (71) Wang, H.; Li, X.; Li, P.; Yang, J. δ -phosphorene: a two dimensional material with a highly negative Poisson's ratio. *Nanoscale* **2017**, *9*, 850–855.
- (72) Jiang, J.-W.; Park, H. S. Negative Poisson's ratio in single-layer graphene ribbons. *Nano Lett.* **2016**, *16*, 2657–2662.
- (73) Shaat, M.; Wagih, A. Hinged-3D metamaterials with giant and strain-independent Poisson's ratios. *Sci. Rep.* **2020**, *10*, 2228.
- (74) Huang, L.; Callan, J. P.; Glezer, E. N.; Mazur, E. GaAs under intense ultrafast excitation: response of the dielectric function. *Phys. Rev. Lett.* **1998**, *80*, 185–188.
- (75) Yakuphanoglu, F. Electrical conductivity, seebeck coefficient and optical properties of SnO₂ film deposited on ITO by dip coating. *J. Alloys Compd.* **2009**, *470*, 55–59.
- (76) Painter, O.; Lee, R. K.; Scherer, A.; Yariv, A.; O'Brien, J. D.; Dapkus, P. D.; Kim, I. Two-dimensional photonic band-gap defect mode laser. *Science* **1999**, *284*, 1819–1821.